Effect of the composition and surface functional groups of Fe-Ni bimetal oxides catalysts in catalytic ozonation process

Zhang Gucheng, Zhang Jing, Zhang Yongli, Zhou Peng, Wei Chenmo, Li Wenshu and Chen Liwei

ABSTRACT

In this study, Fe-Ni bimetal oxides (Fe-NiO_x) catalysts were used to activate O_3 in a heterogeneous system. This research focuses on the degradation mechanism of dimethyl phthalate (DMP) by adding Fe-NiO_x catalysts which activated the O_3 decomposition to generate strong oxidative hydroxyl radicals (•OH). The experimental results showed that O_3/Fe-NiO_x catalyst calcinated under 500 °C achieved 47.75% higher DMP removal efficiency when compared with ozonation of DMP without the catalyst. Besides, control experimental data suggested that the adsorption of DMP was negligible (<4%) for Fe-NiO_x. Thus, it was concluded that the removal of DMP was due to the catalytic ability of Fe-NiO_x rather than the adsorption of DMP onto the catalysts. Moreover, the unsatisfactory performance of Fe-NiO_x catalysts calcinated in the presence of N_2 revealed that O_2 played an important part in affecting the crystalline degree of catalysts during the synthesis process. Meanwhile, the X-ray photoelectron spectroscopy (XPS) and Fourier transform infrared spectroscopy (FT-IR) characterization analysis indicated that calcination temperature was an indispensable factor that influenced the relative content of Ni^{2+} and hydroxyl groups (−OH) in Fe-NiO_x catalysts. Furthermore, the relative content of Ni^{2+} had a greater effect on catalysts' activity because of the electron transfer between multivalent metal states.

Key words | bimetallic oxides, dimethyl phthalate, hydroxyl radicals, ozone, nickel ferrite

Zhang Gucheng
Zhang Jing
Zhang Yongli (corresponding author)
Zhou Peng
Wei Chenmo
Li Wenshu
College of Architecture & Environment,
Sichuan University,
610065 Chengdu, Sichuan,
China
E-mail: *xyl_scu@126.com*

Chen Liwei
College of Biology and the Environment,
Nanjing Forestry University,
Nanjing 210037, Jiangsu,
China

INTRODUCTION

Nowadays, organic pollutants in wastewater are so complex that it is difficult to remove them by traditional water treatment methods. Some organic pollutants in wastewater may increase health risks when discharged to natural water systems due to their toxicity and persistence (Maddila *et al.* 2014). Aiming to degrade various organic contaminants, advanced oxidation processes (AOPs) have been investigated extensively by using a series of physical chemistry methods to activate ozone, peroxide, persulfate, and peroxymonosulfate to produce reactive radicals, such as hydroxyl radicals (•OH) and sulfate radicals ($\bullet SO_4^-$).

Recently, heterogeneous catalytic ozonation has attracted increasing attention owing to its potential higher effectiveness in degrading refractory organic pollutants and lower negative influence on water quality (Trapido *et al.* 1997; Xing *et al.* 2008; Maddila *et al.* 2013; Nie *et al.* 2014). It can be directly applied in real water treatment without any auxiliary thermal or light set-up by adding catalysts into a reaction system in order to enhance the generation of hydroxyl radicals (•OH), the less selective oxidants (Andreozzi *et al.* 1996; Legube & Leitner 1999).

Based on previous research, metal elements are commonly used to prepare solid catalysts for heterogeneous

doi: 10.2166/aqua.2018.116

systems because metal oxides can be easily separated from reactant water making it more applicable for practical applications (Sanchez-Polo *et al.* 2006). As a whole, iron, nickel, copper, and cobalt, etc., are the most common elements used to prepare catalysts (Pines & Reckhow 2003; Zhao *et al.* 2009; Yuan *et al.* 2016). For instance, TiO_2, ZnO and MnO_2 have shown excellent catalytic performance in catalytic ozonation (Song *et al.* 2010). Therefore, the combination of different metal elements to improve the activity of metal oxide catalysts has attracted researchers' attention. According to previous literatures, the application of bimetallic oxides during the ozonation process is remarkable. Bimetal catalysts, such as Ce-V, Pd-Ce and Fe-Ni, all have high potential in dechlorination or catalysis of ozone and peroxymonosulfate due to their special bimetallic structure (Li *et al.* 2012; Ren *et al.* 2012; Maddila *et al.* 2014; Ren *et al.* 2015). Moreover, it is reported that the composition and surface groups are changed with different preparation conditions during the synthesis process (Chan & Barteau 2005; de Diego *et al.* 2005; Mazille *et al.* 2009).

In this study, the effect of calcination temperature of Fe-Ni bimetal oxides (Fe-NiO_x) catalysts and the interaction among catalysts, dimethyl phthalate (DMP) and ozone (O_3) were analyzed. DMP was selected as the probe to evaluate the property of the catalysts. The composition and chemical state of different Fe-NiO_x catalysts were identified by powder X-ray diffraction (XRD) and X-ray photoelectron spectroscopy (XPS), respectively. The surface groups were investigated in detail by Fourier transform infrared spectroscopy (FT-IR) while the effect of temperature was determined by thermal gravity analysis (TGA) and derivative thermogravimetric analysis (DTA).

METHODS

DMP was purchased from Sigma-Aldrich (USA). Nickel nitrate ($Ni(NO_3)_2{\cdot}6H_2O$), ferric nitrate ($Fe(NO_3)_3{\cdot}9H_2O$), tert-butyl alcohol (TBA), sodium dihydrogen phosphate ($NaH_2PO_4{\cdot}2H_2O$), disodium hydrogen phosphate ($Na_2HPO_4{\cdot}12H_2O$) and sodium sulfate (Na_2SO_3) were obtained from Chengdu Kelong Chemical Reagent Company (Chengdu, China). The fresh eggs were bought from a local market (Chengdu, China). All chemicals were analytical grade and the experimental solutions were prepared with ultra-pure water. The solution pH was adjusted by NaH_2PO_4-Na_2HPO_4 buffer.

Fe-NiO_x catalysts were prepared by the sol-gel process with egg white (Maensiri *et al.* 2007; Ren *et al.* 2012). Aqueous solution of nickel nitrate and ferric nitrate was slowly added into fresh egg white with constant stirring. The sol mixture was heated by a water bath at 80 °C for half an hour and then placed in a furnace until the dried precursor was obtained. The dried precursor was ground up and calcinated for 2 hours by blowing air. Finally, the product was crushed into powder by agate mortar. Catalysts were calcinated at 400, 500, and 600 °C with mol ratio $c(Fe^{3+})$: $c(Ni^{2+}) = 1{:}4$.

The composition of metal oxides in catalysts was observed by XRD using a DX-1000 diffract meter. The chemical state of elements was analyzed by Auger electron spectroscopy with a XSAM 800 system. Surface elemental stoichiometry was determined from XPS spectral area ratios. Surface groups on catalysts were identified by FT-IR which was recorded on a Nicolet 6700 spectrometer in the range of 400–4,000 cm^{-1} using the KBr disk method. The influence of temperature was investigated by TGA using a Mettler Toledo TGA/DSC2 and the heating rate was 10 °C/min.

The ozonation experiments were performed at room temperature (18 ± 1 °C) in a 500 mL flat-bottomed flask. Ozone was synthesized by an ozone generator (HTU-500SE, Azco Industries Limited, Canada) using dry oxygen as the supply gas. The ozone concentration in water was determined using a UV-vis spectrophotometer (UV-1800, Mapada Instruments, China) (Valdes *et al.* 2008). The pH was adjusted to 7.1 by phosphate buffer. Then 0.05 g catalyst powder and 0.5 mL DMP stock solution (440 mg/L) were immediately added to the ozone solution (0.5 mg/L). A magnetic stirrer was used to ensure maximum contact of substrates. Samples were immediately quenched into excess Na_2SO_3 solution to remove residual ozone after withdrawal from the reactor at different time intervals.

The concentration of DMP was analyzed by a high-performance liquid chromatograph (HPLC, Waters e2695) equipped with a Waters C18 column and UV detector at 228 nm. The mobile phase (1.0 mL/min) was a mixture of methanol and ultra-pure water (V/V = 50/50). The

experiments aiming to investigate O_3 decomposition were carried out under the same control conditions without DMP in the system. At given time intervals, the concentration of residual ozone in the aqueous solution was measured using the indigo method (Bader & Hoigne 1981).

RESULTS AND DISCUSSION

XPS characterization

Figure 1 shows the XPS spectra of Fe (a), Ni (b) and O (c) in catalysts calcinated at 400, 500, and 600 °C before and after ozonation. The binding energy at 710.9 and 724.8 eV in Figure 1(a) was assigned to $NiFe_2O_4$ (Ren *et al.* 2012). As there was no significant change after the reaction, the results indicated that the iron ion did not experience redox reaction.

In Figure 1(b), the high-resolution Ni2p spectra displayed Ni^{3+} at 861.4 eV and Ni^{2+} at 855.4 eV (Wang *et al.* 2010; Ren *et al.* 2012). Catalysts calcinated at 500 °C with air had the highest ratio of Ni^{2+} before reaction and it decreased from 74.26% to 49.31% after reaction. The change between Ni^{2+} and Ni^{3+} could have resulted from the oxidation condition provided by O_3 in the system (Ren *et al.* 2015). The electron transfer between Ni^{2+} and Ni^{3+} which indicated the involvement of the Ni^{2+}–Ni^{3+}–Ni^{2+} redox process during the reaction explained the reason why the catalysts could enhance catalytic ozonation (Ren *et al.* 2012).

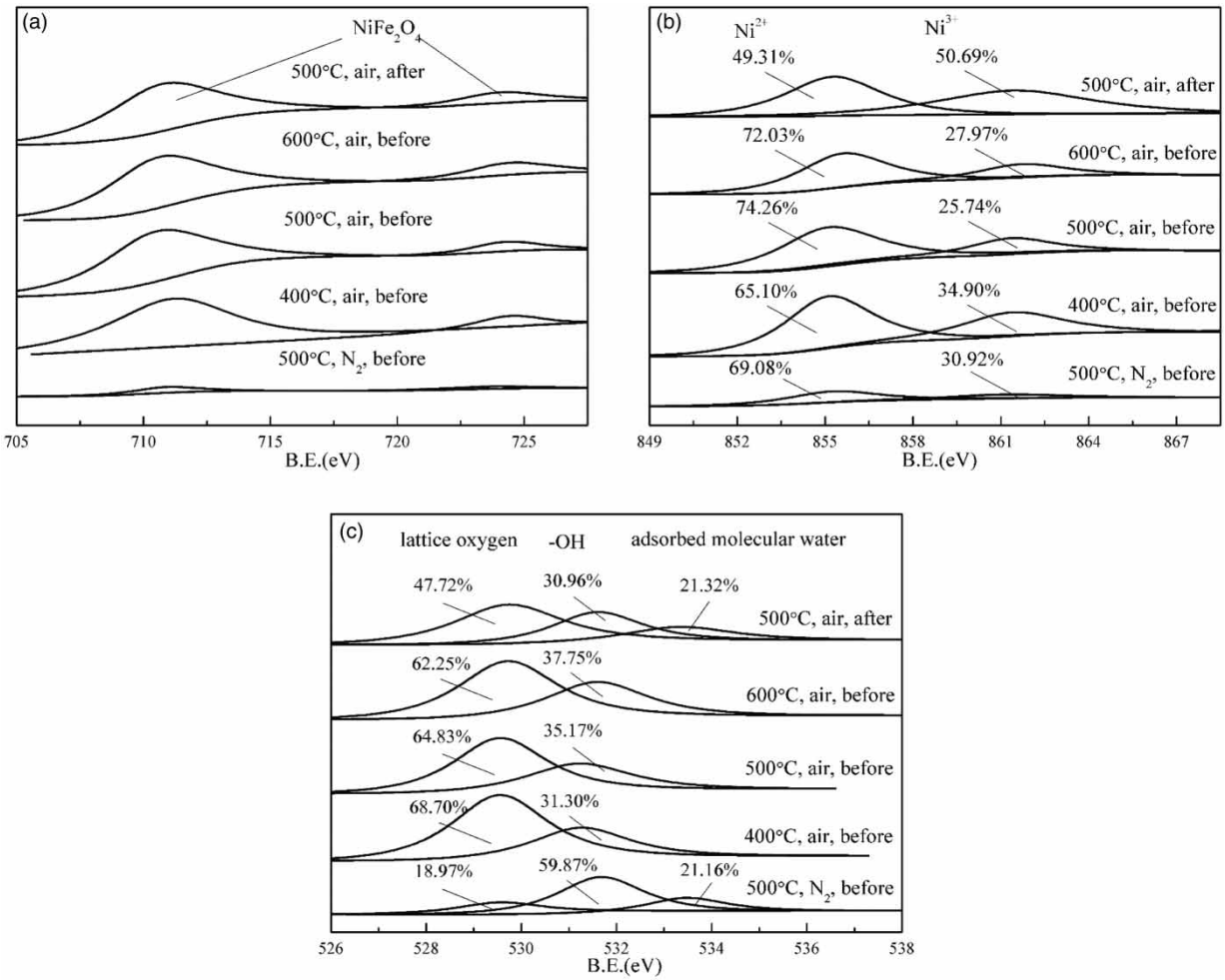

Figure 1 | XPS spectra of different catalysts before and after experiments: (a) Fe, (b) Ni, (c) O.

From Figure 1(c), it was revealed that O1s spectra was characterized with three peaks: the peak at the lower binding energy (529.4–530.0 eV) was ascribed to lattice oxygen; the peak at 531.25–531.8 eV was assigned to the hydroxyl groups (−OH) and the peak at the higher binding energy (above 533.0 eV) was associated with adsorbed molecular water (Machocki *et al.* 2004; Dai *et al.* 2012). The ratio of −OH in catalysts with air blown rose from 30.30% to 37.75%, when calcination temperature increased. After reaction, the ratio in the catalysts calcinated under 500 °C decreased from 35.17% to 30.96% and a new peak appeared due to adsorbed molecular water.

Overall, the Figure 1 results showed that though the relative ratio of −OH in the catalysts calcinated at 500 °C by blowing N_2 was very high, all peaks were much weaker, which suggested that there were less metal oxides in the catalysts. Thus, it could be inferred that O_2 played an important role in the formation of $NiFe_2O_4$ and −OH.

TGA characterization

In order to investigate the effect of temperature of catalysts on its decomposition and crystallization, the precursor was subjected to TGA-DTA. In Figure 2, continuous weight loss is shown, owing to the combustion of the organic matter and the loss of trapped water in the egg white during the catalysts synthesis. The peaks of the DTA curve were observed when the organic matter in the precursor burnt out (Maensiri *et al.* 2007). When the temperature rose to 600 °C, the wave disappeared because all the organic matter was burnt out.

XRD characterization

The XRD pattern of all Fe-NiO_x catalysts is shown in Figure 3. It shows that catalysts calcinated at 500 and 600 °C had $NiFe_2O_4$, NiO and Ni_2O_3 phases. And the peaks at $2\theta = 37.4°$, 43.4° and 63.1° were sharper under rising calcination temperature, which suggested that Fe-Ni mixed oxides were crystallized better (Muruganandham & Wu 2008). However, the catalysts synthesized at 500 °C under N_2 atmosphere had weaker intensity of peaks because the combustion of organic matter in the precursor was incomplete in the absence of O_2. To combine with Figure 1 though, the ratio of every phase was nearly the same, the different crystalline degree of catalysts under various calcination temperatures influenced the catalytic performance. Thus, it was proved that calcination temperature affected the crystalline state of metal oxides and O_2 played an important role in their formation process.

FT-IR characterization

Figure 4 reveals the FT-IR spectra of catalysts calcinated at 400, 500 and 600 °C before experiments. Three hydroxyl group absorption bands emerged in all curves. The first peak was at 3,425 cm^{-1}, corresponding to the stretching of

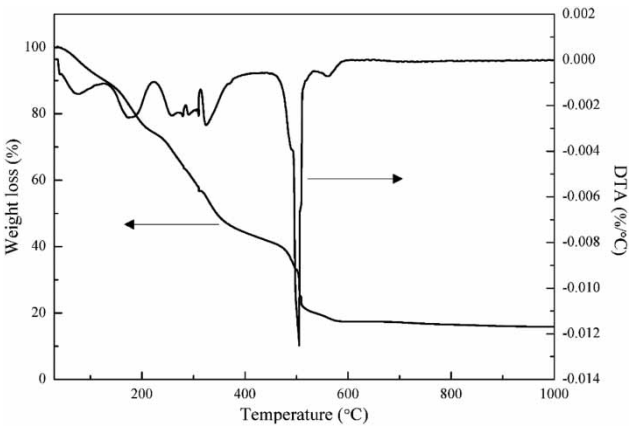

Figure 2 | TGA-DTA curves of precursor.

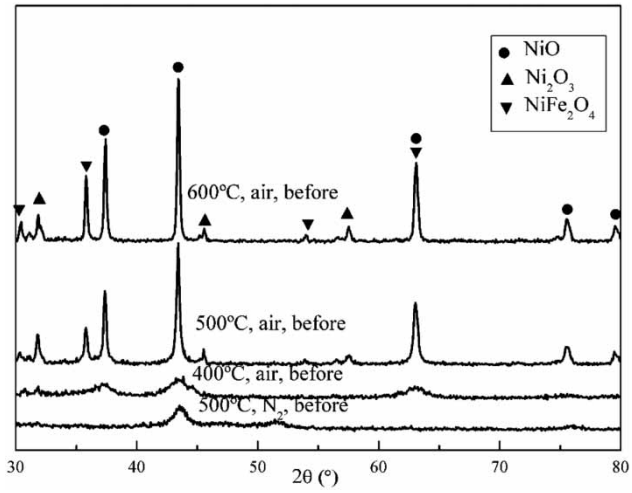

Figure 3 | XRD patterns of different catalysts before and after experiments.

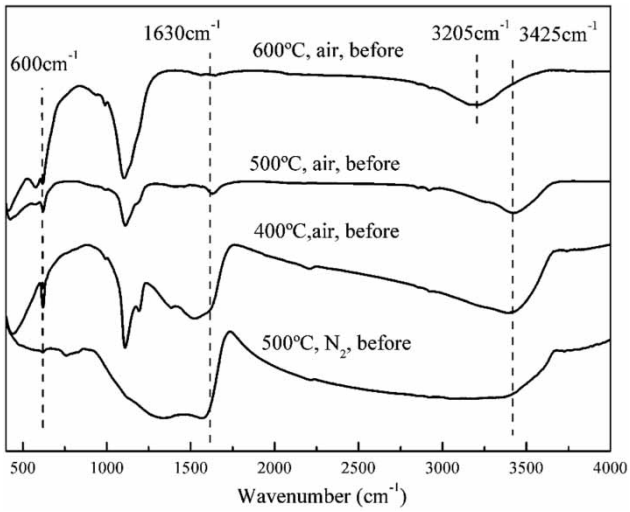

Figure 4 | FT-IR spectra of different catalysts before experiments.

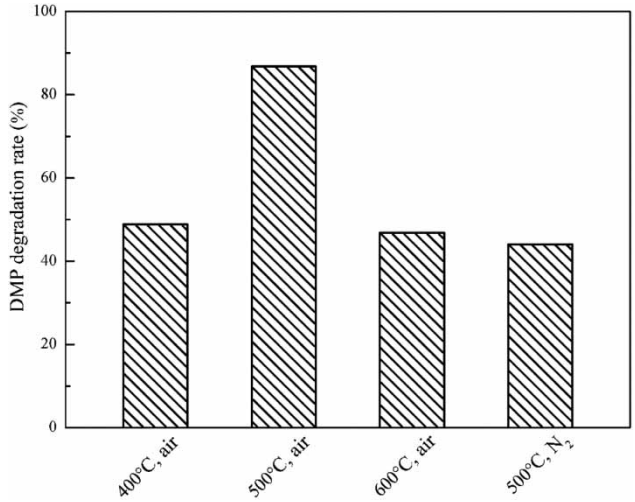

Figure 5 | DMP degradation rates with different catalysts.

the hydrogen-bounded M-OH (M: Fe and Ni) (Lv *et al.* 2010; Zhao *et al.* 2015). The second peak was between 1,628 and 1,640 cm^{-1} due to the bending vibrations of the associated water (Maddila *et al.* 2014) and the third peak was at nearly 3,205 cm^{-1} reflecting the hydrogen-bonded water (Zhao *et al.* 2014). Additionally, the absorption band around 600 cm^{-1} corresponded to the intrinsic stretching variations of metal elements at tetrahedral sites in $NiFe_2O_4$ (Florea *et al.* 2009). In contrast, the peak intensities of catalysts prepared with N_2 were weaker, which indicated that O_2 had a significant impact on the formation of surface groups.

Catalytic ability of Fe-NiO_x oxides

The catalytic activity experiments within 10 min were carried out with different catalysts and the results are presented in Figure 5. It is noted that the removal efficiency of DMP was significantly enhanced with the addition of Fe-NiO_x catalysts calcinated at 500 °C, which achieved nearly 86.83% DMP degraded in 10 min in the Fe-NiO_x/O_3/DMP system. Only 47% and 46% DMP was degraded with catalysts calcinated at 400 °C and 600 °C under the same experimental conditions. Meanwhile, approximately 44% of DMP was removed during the ozonation process activated by the catalysts prepared with N_2.

Both results of catalysts calcinated at 400 and 500 °C in Figures 3 and 4 indicated that the better crystalline degree of catalysts led to more DMP being degraded. Besides, results of catalysts calcinated at 500 and 600 °C in XPS analysis showed that the catalysts calcinated at 500 °C had more Ni^{2+} which contributed to stronger catalytic power on O_3 activation.

As has been well proven in previous studies, the relationship between catalytic ability and density of −OH on the catalysts surface had a positive linear correlation. To be more specific, −OH reacted with O_3, generating unstable species as the promoter of O_3 chain decomposition and, thus, produced •OH (Yang *et al.* 2007; Zhang *et al.* 2008; Sui *et al.* 2012). Multivalence oxidation states improved interfacial electron transfer which made the organic pollutant degrade rapidly (Xing *et al.* 2008; Lv *et al.* 2010). Therefore, it could be inferred that Fe-NiO_x oxides could catalyze the ozonation process because of the interaction of multivalent Ni and −OH. However, this research result contradicted previous ones which insisted that more −OH led to better degradation results in heterogeneous catalytic process (Yang *et al.* 2007; Zhang *et al.* 2008; Sui *et al.* 2012; Zhao *et al.* 2015). The Ni^{2+}-Ni^{3+} redox process in the system and the electron transfer between them which enhanced the oxidation reaction had led to this phenomenon (Ren *et al.* 2012).

Ozone decomposition with Fe-NiO_x oxides

A series of ozone decomposition experiments was carried out with various catalysts. As shown in Figure 6, all catalysts

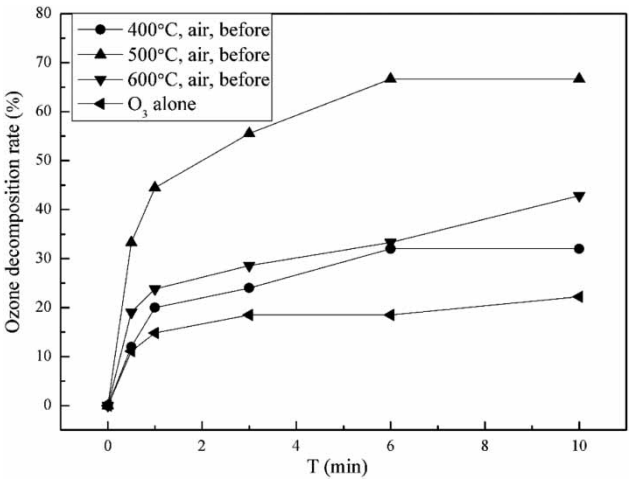

Figure 6 | Ozone decomposition rate with different catalysts.

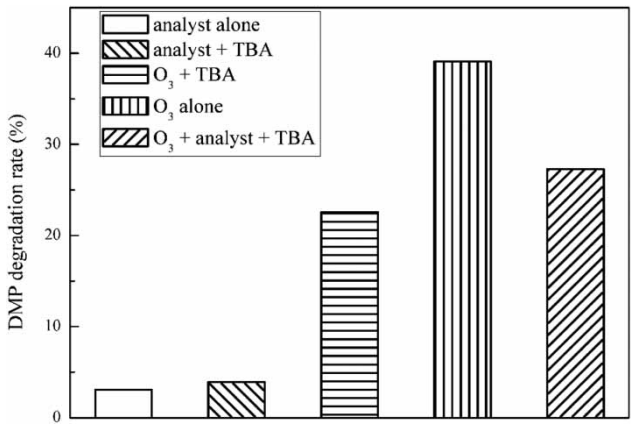

Figure 7 | DMP degradation rate with TBA.

significantly promoted ozone decomposition compared to the rate of the O_3 alone system. As the ozone decomposition results followed a similar pattern in Figure 5, catalysts calcinated at 500 °C by blowing air were the most effective with nearly 66.67% O_3 decomposed. Reactive species generated from O_3 chain decomposition were not consumed without pollutant in the system in Figure 5 and this might narrow the rate difference between O_3 decomposition in Figures 5 and 6 (Lv *et al.* 2010; Zhao *et al.* 2015).

Active oxidative species in ozonation system

The improvement in DMP degradation was ascribed to the formation of active oxidative species with O_3 decomposed, which had high oxidative ability to remove refractory organic matter (Yang *et al.* 2009; Huang *et al.* 2011; Zhao *et al.* 2013). In order to confirm whether •OH was generated or not during the AOP, TBA was used as radical scavenger because its reaction rate constant with •OH is $6 \times 10^8\ M^{-1}\ s^{-1}$ and with O_3 it is only $3 \times 10^{-3}\ M^{-1}\ s^{-1}$ (Acero *et al.* 2001).

As shown in Figure 7, after adding TBA, DMP degradation was significantly inhibited from 86.83% to 27.29% in 10 min with both O_3 and the catalysts calcinated at 500 °C by blowing air in the system. Since TBA had a much higher reaction rate constant with •OH than O_3, the decrease was due to the consumption of •OH caused by TBA. About 39.08% DMP was degraded in 10 min with O_3 alone and it decreased to 22.57% with the addition of TBA. Besides, only adding catalysts into the system resulted in less than 4% DMP being adsorbed with or without TBA experimental conditions.

CONCLUSIONS

Calcination temperature and O_2 were important factors which influenced the crystalline degree and relative content of Ni^{2+} and −OH during the Fe-NiO_x catalysts synthesis process. Different calcination temperatures led to different precursor decomposition and crystalline process, and O_2 affected the oxidation level of organic matter in the precursor. The beneficial effect on DMP degradation was promoted by the Ni^{2+}-Ni^{3+} redox process and −OH. The presence of Ni^{2+} had a much stronger impact because the electron transfer between multivalence could accelerate O_3 decomposition and •OH generation. The degradation process was mainly attributed to the presence of •OH generated from the process of O_3 activated by Fe-NiO_x catalysts, while the adsorption of DMP could be ignored.

ACKNOWLEDGEMENTS

Appreciation and acknowledgment are given to the National Natural Science Foundation of China (No. 51508353), Natural Science Foundation of Jiangsu Province (BK201409660) and the National Science

Foundation of the Higher Education Institutions of Jiangsu Province of China (14KJB610006).

REFERENCES

Acero, J. L., Haderlein, S. B., Schmidt, T. C., Suter, M. J. F. & von Gunten, U. 2001 MTBE oxidation by conventional ozonation and the combination ozone/hydrogen peroxide: efficiency of the processes and bromate formation. *Environmental Science & Technology* **35** (21), 4252–4259.

Andreozzi, R., Insola, A., Caprio, V., Marotta, R. & Tufano, V. 1996 The use of manganese dioxide as a heterogeneous catalyst for oxalic acid ozonation in aqueous solution. *Applied Catalysis A: General* **138** (1), 75–81.

Bader, H. & Hoigne, J. 1981 Determination of ozone in water by the indigo method. *Water Research* **15** (4), 449–456.

Chan, S. C. & Barteau, M. A. 2005 Preparation of highly uniform Ag/TiO_2 and Au/TiO_2 supported nanoparticle catalysts by photodeposition. *Langmuir* **21** (12), 5588–5595.

Dai, Y., Wang, X., Dai, Q. & Li, D. 2012 Effect of Ce and La on the structure and activity of MnOx catalyst in catalytic combustion of chlorobenzene. *Applied Catalysis B: Environmental* **111–112**, 141–149.

de Diego, L. F., Gayán, P., García-Labiano, F., Celaya, J., Abad, A. & Adánez, J. 2005 Impregnated CuO/Al_2 O_3 oxygen carriers for chemical-looping combustion: avoiding fluidized bed agglomeration. *Energy & Fuels* **19** (5), 1850–1856.

Florea, M., Alifanti, M., Parvulescu, V. I., Mihaila-Tarabasanu, D., Diamandescu, L., Feder, M., Negrila, C. & Frunza, L. 2009 Total oxidation of toluene on ferrite-type catalysts. *Catalysis Today* **141** (3–4), 361–366.

Huang, R., Yan, H., Li, L., Deng, D., Shu, Y. & Zhang, Q. 2011 Catalytic activity of Fe/SBA-15 for ozonation of dimethyl phthalate in aqueous solution. *Applied Catalysis B: Environmental* **106** (1–2), 264–271.

Legube, B. & Leitner, N. 1999 Catalytic ozonation: a promising advanced oxidation technology for water treatment. *Catalysis Today* **53** (1), 61–72.

Li, W., Qiang, Z., Zhang, T. & Cao, F. 2012 Kinetics and mechanism of pyruvic acid degradation by ozone in the presence of PdO/CeO_2. *Applied Catalysis B: Environmental* **113–114** (1–2), 290–295.

Lv, A., Hu, C., Nie, Y. & Qu, J. 2010 Catalytic ozonation of toxic pollutants over magnetic cobalt and manganese co-doped γ-Fe_2O_3. *Applied Catalysis B: Environmental* **100** (1–2), 62–67.

Machocki, A., Ioannides, T., Stasinska, B., Gac, W., Avgouropoulos, G., Delimaris, D., Grzegorczyk, W. & Pasieczna, S. 2004 Manganese-lanthanum oxides modified with silver for the catalytic combustion of methane. *Journal of Catalysis* **227** (2), 282–296.

Maddila, S., Dasireddy, V. D. B. C. & Jonnalagadda, S. B. 2013 Dechlorination of tetrachloro-o-benzoquinone by ozonation catalyzed by cesium loaded metal oxides. *Applied Catalysis B: Environmental* **138**, 149–160.

Maddila, S., Dasireddy, V. D. B. C. & Jonnalagadda, S. B. 2014 Ce-v loaded metal oxides as catalysts for dechlorination of chloronitrophenol by ozone. *Applied Catalysis B: Environmental* **150–151**, 305–314.

Maensiri, S., Masingboon, C., Boonchom, B. & Seraphin, S. 2007 A simple route to synthesize nickel ferrite ($NiFe_2O_4$) nanoparticles using egg white. *Scripta Materialia* **56** (9), 797–800.

Mazille, F., Schoettl, T. & Pulgarin, C. 2009 Synergistic effect of TiO_2 and iron oxide supported on fluorocarbon films. Part 1: effect of preparation parameters on photocatalytic degradation of organic pollutant at neutral ph. *Applied Catalysis B: Environmental* **89** (3–4), 635–644.

Muruganandham, M. & Wu, J. J. 2008 Synthesis, characterization and catalytic activity of easily recyclable zinc oxide nanobundles. *Applied Catalysis B: Environmental* **80** (1–2), 32–41.

Nie, Y., Hu, C., Li, N., Yang, L. & Qu, J. 2014 Inhibition of bromate formation by surface reduction in catalytic ozonation of organic pollutants over beta-$FeOOH/Al_2O_3$. *Applied Catalysis B: Environmental* **147**, 287–292.

Pines, D. S. & Reckhow, D. A. 2003 Solid phase catalytic ozonation process for the destruction of a model pollutant. *Ozone Science & Engineering* **25** (1), 25–39.

Ren, Y., Dong, Q., Feng, J., Ma, J., Wen, Q. & Zhang, M. 2012 Magnetic porous ferrospinel $NiFe_2O_4$: a novel ozonation catalyst with strong catalytic property for degradation of di-n-butyl phthalate and convenient separation from water. *Journal of Colloid and Interface Science* **382** (1), 90–96.

Ren, Y., Lin, L., Ma, J., Yang, J., Feng, J. & Fan, Z. 2015 Sulfate radicals induced from peroxymonosulfate by magnetic ferrospinel MFe_2O_4 (M = Co, Cu, Mn, and Zn) as heterogeneous catalysts in the water. *Applied Catalysis B: Environmental* **165**, 572–578.

Sanchez-Polo, M., Rivera-Utrilla, J. & von Gunten, U. 2006 Metal-doped carbon aerogels as catalysts during ozonation processes in aqueous solutions. *Water Research* **40** (18), 3375–3384.

Song, S., Liu, Z., He, Z., Zhang, A., Chen, J., Yang, Y. & Xu, X. 2010 Impacts of morphology and crystallite phases of titanium oxide on the catalytic ozonation of phenol. *Environmental Science & Technology* **44** (10), 3913–3918.

Sui, M., Xing, S., Sheng, L., Huang, S. & Guo, H. 2012 Heterogeneous catalytic ozonation of ciprofloxacin in water with carbon nanotube supported manganese oxides as catalyst. *Journal of Hazardous Materials* **227**, 227–236.

Trapido, M., Hirvonen, A., Veressinina, Y., Hentunen, J. & Munter, R. 1997 Ozonation, ozone/UV and UV/H_2O_2 degradation of chlorophenols. *Ozone Science & Engineering* **19** (1), 75–96.

Valdes, H., Murillo, F., Manoli, J. & Zaror, C. 2008 Heterogeneous catalytic ozonation of benzothiazole aqueous solution promoted by volcanic sand. *Journal of Hazardous Materials* **153** (3), 1036–1042.

Wang, Z.-Y., Chou, H.-C., Wu, J. C. S., Tsai, D. P. & Mul, G. 2010 CO2 photoreduction using NiO/InTaO4 in optical-fiber reactor for renewable energy. *Applied Catalysis A: General* **380** (1–2), 172–177.

Xing, S., Hu, C., Qu, J., He, H. & Yang, M. 2008 Characterization and reactivity of MnOx supported on mesoporous zirconia for herbicide 2,4-d mineralization with ozone. *Environmental Science & Technology* **42** (9), 3363–3368.

Yang, Y., Ma, J., Qin, Q. & Zhai, X. 2007 Degradation of nitrobenzene by nano-tio$_2$ catalyzed ozonation. *Journal of Molecular Catalysis A: Chemical* **267** (1–2), 41–48.

Yang, L., Hu, C., Nie, Y. & Qu, J. 2009 Catalytic ozonation of selected pharmaceuticals over mesoporous alumina-supported manganese oxide. *Environmental Science & Technology* **43** (7), 2525–2529.

Yuan, L., Shen, J., Chen, Z. & Guan, X. 2016 Role of Fe/pumice composition and structure in promoting ozonation reactions. *Applied Catalysis B: Environmental* **180**, 707–714.

Zhang, T., Li, C., Ma, J., Tian, H. & Qiang, Z. 2008 Surface hydroxyl groups of synthetic alpha-FeOOH in promoting (OH)-O-center dot generation from aqueous ozone: property and activity relationship. *Applied Catalysis B: Environmental* **82** (1–2), 131–137.

Zhao, L., Sun, Z. & Ma, J. 2009 Novel relationship between hydroxyl radical initiation and surface group of ceramic honeycomb supported metals for the catalytic ozonation of nitrobenzene in aqueous solution. *Environmental Science & Technology* **43** (11), 4157–4163.

Zhao, H., Dong, Y., Wang, G., Jiang, P., Zhang, J., Wu, L. & Li, K. 2013 Novel magnetically separable nanomaterials for heterogeneous catalytic ozonation of phenol pollutant: NiFe2O4 and their performances. *Chemical Engineering Journal* **219**, 295–302.

Zhao, H., Dong, Y., Jiang, P., Wang, G., Zhang, J., Li, K. & Feng, C. 2014 An α-MnO2 nanotube used as a novel catalyst in ozonation: performance and the mechanism. *New Journal of Chemistry* **38** (4), 1743–1750.

Zhao, H., Dong, Y., Jiang, P., Wang, G., Zhang, J. & Zhang, C. 2015 $ZnAl_2O_4$ as a novel high-surface-area ozonation catalyst: one-step green synthesis, catalytic performance and mechanism. *Chemical Engineering Journal* **260**, 623–630.

First received 19 July 2017; accepted in revised form 1 January 2018. Available online 29 January 2018